ADVANCED FUNCTIONAL MATERIALS
www.afm-journal.de

A Novel Carbazolophane: A Comparison of the Performance of Two Planar Chiral CP-TADF Emitters

Jasmin Seibert, Yan Xu, Hassan Hafeez, Joachim Podlech, Ludovic Favereau, Eduard Spuling, Charlotte Waldhelm, Martin Nieger, Olaf Fuhr, Zahid Hassan, Jeanne Crassous, Ifor D. W. Samuel, Eli Zysman-Colman,* and Stefan Bräse**

The prototypical example of a (cyclo)phane, [2.2]paracyclophane (PCP), has proven to be a versatile stereogenic moiety within the design of circularly polarized thermally activated delayed fluorescence (CP-TADF) emitters; however, the exploration of other cyclophanes within CP-TADF emitter design has been largely neglected. Here, a comparative study of the photophysical and optoelectronic properties of two cyclophane emitters, (1,7)*t*BuCzpPhTrz and its isomer (1,4)*t*BuCzpPhTrz, is presented. The carbazolophane-triazine compound (1,7)*t*BuCzpPhTrz, obtained via an unprecedented intramolecular rearrangement, is the first example of a planar chiral TADF emitter deviating from the PCP scaffold. Significant geometrical change of the enclosed carbazole in (1,7)*t*BuCzp results in an attenuation of the donor strength, while the merits of rigidity and steric bulk remain. In particular, the full width at half maximum (FWHM) of the photoluminescence spectrum in toluene of (1,7)*t*BuCzpPhTrz is reduced by 34% and blue-shifted by 20 nm compared to that of (1,4)*t*BuCzpPhTrz. In doped films, the compounds reach high photoluminescence quantum yields (Φ_{PL}) of 91 and 81%, respectively. The chiroptical properties reveal dissymmetry factors $|g_{PL}|$ of up to 5×10^{-4}. These results demonstrate the impact of the cyclophane for the development of CP-TADF materials and add to the currently limited scope of available planar chiral donors.

1. Introduction

Compounds exhibiting thermally activated delayed fluorescence (TADF) show a dual emission where a prompt fluorescence originates from rapid radiative decay of singlet excitons and a delayed fluorescence follows the endothermic up-conversion of non-emissive triplet excitons to singlets. This reverse intersystem crossing (RISC) is exploited in organic light-emitting diodes (OLEDs), which can then reach an internal quantum efficiency (IQE) of up to 100%, making organic TADF materials desired targets for electroluminescent device applications.[1] TADF emitter design produces organic semiconductors that possess a suitably small energy gap, ΔE_{ST}, between the first excited singlet (S_1) and triplet (T_1) excited states. The most prominent design are compounds that have a strongly twisted donor-acceptor (D-A) structure wherein the electron density in the highest occupied molecular orbital (HOMO) is mainly localized on the

J. Seibert, J. Podlech, E. Spuling, C. Waldhelm, Z. Hassan, S. Bräse
Institute of Organic Chemistry (IOC)
Karlsruhe Institute of Technology (KIT)
Kaiserstrasse 12, 76131 Karlsruhe, Germany
E-mail: braese@kit.edu

Y. Xu, E. Zysman-Colman
Organic Semiconductor Centre, EaStCHEM School of Chemistry
University of St Andrews
St Andrews, Fife KY16 9ST, UK
E-mail: eli.zysman-colman@st-andrews.ac.uk

H. Hafeez, I. D. W. Samuel
Organic Semiconductor Centre, SUPA School of Physics and Astronomy
University of St Andrews
St Andrews, Fife KY16 9SS, UK
E-mail: idws@st-andrews.ac.uk

L. Favereau, J. Crassous
CNRS, ISCR (Institut des Sciences Chimiques de Rennes) – UMR 6226
University of Rennes
Rennes F-35000, France

M. Nieger
Department of Chemistry
00014 University of Helsinki
P. O. Box 55 (A. I. Virtasen aukio 1), Helsinki Finland

O. Fuhr
Institute of Nanotechnology (INT) and Karlsruhe Nano-Micro Facility (KNMFi)
Karlsruhe Institute of Technology (KIT)
Kaiserstrasse 12, 76131 Karlsruhe, Germany

S. Bräse
Institute of Biological and Chemical Systems (IBCS-FMS)
Karlsruhe Institute of Technology (KIT)
Kaiserstrasse 12, 76131 Karlsruhe, Germany

The ORCID identification number(s) for the author(s) of this article can be found under https://doi.org/10.1002/adfm.202401956

DOI: 10.1002/adfm.202401956

donor moiety while the lowest unoccupied molecular orbital (LUMO) is found on the electron-withdrawing acceptor, leading to a small exchange integral and thus a small ΔE_{ST} that is essential for TADF.[1a]

OLEDs face a trade-off between high contrast ratios, achieved by reducing reflection of incident light, and brightness loss, when ≈50% of the produced light from the emissive layer is absorbed by anti-glare filters that are present in most of these devices. These filters convert unpolarized light into circularly polarized (CP) light (CPL). Upon reflection, the polarization of the CPL is reversed, preventing it from passing the filter; however, besides the suppression of the reflected incident light, the generated light of the OLED is also trapped. A strategy to circumvent this loss channel is to use a material with inherent CPL, thus making anti-glare filters redundant. A quantification of the degree of CPL is the photoluminescence dissymmetry factor $|g_{PL}|$, which can have a maximum value of 2. Most closed-shell organic emitters, however, have very low $|g_{PL}|$, on the order of 10^{-3}.[2] Thus, to achieve optimal results in a device requires employing an emitter that simultaneously can harvest both singlet and triplet excitons to produce light, is bright (i.e., has a high photoluminescence quantum yield, Φ_{PL}), and that the light emanating be CP.

One strategy to design CPL-active materials is to incorporate a planar chiral motif within the emitter design.[3] Among such well-studied motifs are the (cyclo)phanes, a class of cyclic compounds featuring at least one bridged arene. The [2.2]paracyclophane (PCP), a prototypical example consisting of two closely stacked benzene rings, has been at the center of scientific attention, and has proven useful *inter alia* in catalysis,[4] π-conjugated oligomers,[5] porous frameworks,[6] chemical vapour deposition (CVD) coatings,[7] and other material applications.[8] In 2018, we were the first to incorporate this three-dimensional scaffold within a CP-TADF emitter.[9] Decorating the decks with donor (D) and acceptor (A) units produced a material that possessed low-lying charge transfer (CT) excited states whose electronic communication was mediated through the π-stacked core of the PCP. Both isomers, ***cis***- and ***trans*-Bz-PCP-TPA**, showed blue TADF with photoluminescence maxima, λ_{PL}, at 480 nm and 465 nm, respectively in 15 wt% doped films in 1,3-bis(*N*-carbazolyl)benzene (mCP); however, their low Φ_{PL} of 12% and 15% precluded their use as emitters in OLEDs (**Figure 1**).

Zhao and co-workers reported a similar through-space PCP-based emitter **BNMe$_2$-CP** that contained a bulky dimesitylborane acceptor intended to suppress concentration-induced quenching.[10] A hypsochromic shift was observed in toluene for the *pseudo-meta* derivative ***m*-BNMe$_2$-CP** (λ_{PL} = 521 nm) that has the larger D-A distance compared to ***g*-BNMe$_2$-CP** (λ_{PL} = 531 nm). This latter compound has a very short τ_d of 0.38 µs in toluene, a high Φ_{PL} of 72% in cyclohexane and a $|g_{PL}|$ value of 4.2×10^{-3} in toluene. Insertion of an *ortho*-functionalized phenyl moiety produced conformationally more rigid structures ***g*-BPhNMe$_2$-CP**, ***m*-BPhNMe$_2$-CP** and ***m*-BPhNPh$_2$-CP**, emitting at λ_{PL} of 488, 461, and 455 nm and having high Φ_{PL} of 83, 93, and 82%, respectively, in tetrahydrofuran (Figure 1).[11] The $|g_{PL}|$ values were high for organic emitters at 1.3×10^{-2}, 1.7×10^{-2}, and 1.7×10^{-2}, respectively.

The dominant molecular designs for PCP-containing TADF emitters are those with PCP-fused *N*-heterocyclic donors. The [2]paracyclo[2](1,4)carbazolophane (Czp) was introduced as a sterically more demanding and stronger donor that produces emitters with smaller ΔE_{ST} compared to analogues using carbazole (Cz).[12] Compounds **CzpPhTrz**, **CNCzpPhTrz** and **CF$_3$CzpPhTrz** emit at λ_{PL} of 482, 458, and 456 nm and all have high Φ_{PL} of up to 70% in 10 wt% doped films in bis[2-(diphenylphosphino)phenyl] ether oxide (DPEPO) or 2,8-bis(diphenylphosphoryl)dibenzo[*b*,*d*]thiophene (PPT). The enantiomers of **CzpPhTrz** emit CPL with $|g_{PL}|$ of 1.3×10^{-3}.[12b,13] OLEDs with the latter two emitted at λ_{EL} of around 460 nm and showed EQE_{max} of 7.4 and 12%, respectively. The devices suffered from severe efficiency roll-off resulting from the long τ_d of 135 and 158 µs, respectively, and possible degradation as a new emission band at longer wavelength was observed under electrical excitation. The device with **CzpPhTrz** emitted at λ_{EL} of 480 nm and reached an EQE_{max} of 17%. The analogous phenoxazine-derived PCP, **PXZp-Ph-Trz**, has also been reported where the enantiomers emit CPL with $|g_{PL}|$ of 3.3×10^{-3}.[14] The solution-processed CP-OLEDs emitted at λ_{EL} of 560 nm, showed an EQE_{max} of 7.8% and an electroluminescence dissymmetry factor $|g_{EL}|$ of 4.6×10^{-3}. The structurally related emitter **PXZ-PT** contains a PCP that bridges a phenoxazine (PXZ) donor and a triazine acceptor on the same deck. The respective enantiomers emit CPL with $|g_{PL}|$ of 1.9×10^{-3}. The devices emitted at λ_{EL} of 557 nm and showed an EQE_{max} of 20% and $|g_{EL}|$ of 1.5×10^{-3}.[15] Recently, **Czp-*t*BuCzB** and **Czp-POAB** have been reported as the first examples of planar chiral multi-resonance TADF (MR-TADF) emitters, where the Czp donor decorates two known MR-TADF cores. Sky-blue and green CP-TADF devices emitted at λ_{EL} of 479 and 513 nm, and showed EQE_{max} of 32 and 29% and $|g_{EL}|$ of 1.5×10^{-3} and 1.3×10^{-3}.[16] To the best of our knowledge, all planar chiral TADF emitters hitherto rely on the PCP scaffold, while the use of other phane-based moieties is scarce[17] and limited only to larger macrocyclic assemblies, where planar chirality is not present.

Herein, we report the synthesis of a novel carbazolophane class ([2]paracyclo[2] (1,7)carbazolophane) for the design of the cyclophane donor-acceptor TADF emitter **(1,7)*t*BuCzpPhTrz**. Anchored by two ethylene bridges at the 1- and 7-positions, the carbazole unit adopts a convex geometry that engages in π-stacking interactions with the benzene deck of the cyclophane. Its properties are compared to the PCP-fused carbazolophanyl analogue **(1,4)*t*BuCzpPhTrz**. Compound **(1,7)*t*BuCzpPhTrz** has a higher Φ_{PL} of 91% in comparison to 84% for **(1,4)*t*BuCzpPhTrz**. Blue OLEDs showed EQE_{max} of 14 and 17%, respectively, and enantiomerically pure samples of both compounds exhibit similar $|g_{PL}|$ values around 5×10^{-4}.

2. Results and Discussion

2.1. Structural Design and Synthesis

We re-visited earlier works[12,18] on the synthesis of planar chiral carbazole derivatives bearing PCP, and disclose the synthetic route towards **(1,4)*t*BuCzpPhTrz** and **(1,7)*t*BuCzpPhTrz** as outlined in **Scheme 1a**. Both carbazolophane isomers, **(1,7)*t*BuCzp** (**3a**) and **(1,4)*t*BuCzp** (**4a**), were

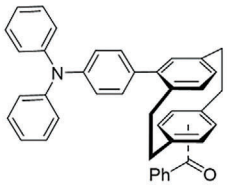

cis-Bz-PCP-TPA | trans-Bz-PCP-TPA
ΔE_{ST} = 0.13 eV, 0.17 eV
τ_d = 1.8 μs, 3.6 μs (15 wt% mCP)
λ_{PL} = 480 nm, 465 nm (15 wt% mCP)
Φ_{PL} = 12%, 15% (PhMe)
Chem. Commun. **2018**, *54*, 9278.

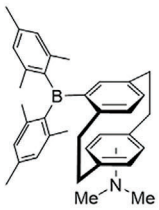

g-BNMe$_2$-CP | m-BNMe$_2$-CP
ΔE_{ST} = 0.17 eV, 0.12 eV
τ_d = 0.38 μs, 0.22 μs (PhMe)
λ_{PL} = 531 nm, 521 nm (PhMe)
Φ_{PL} = 72%, 39% (CyHex)
$|g_{PL}| = 4.2\times10^{-3}$ (PhMe), n.a.
Org. Lett. **2018**, *20*, 6868.

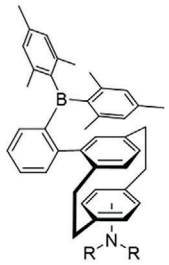

g-BPhNMe$_2$-CP (R=Me) | m-BPhNMe$_2$-CP (R=Me) | m-BPhNPh$_2$-CP (R=Ph)
ΔE_{ST} = n.a., τ_d = n.a.
λ_{PL} = 488 nm, 461 nm, 455 nm (CyHex)
Φ_{PL} = 83%, 93%, 82% (CyHex)
$|g_{PL}| = 1.3\times10^{-2}, 1.7\times10^{-2}, 1.7\times10^{-2}$ (THF)
Org. Lett. **2021**, *23*, 2.

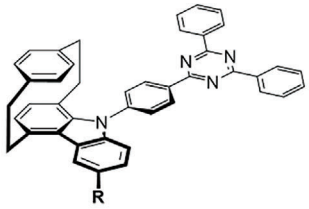

CzpPhTrz (R=H) | CNCzpPhTrz (R=CN) | CF$_3$CzpPhTrz (R=CF$_3$)
ΔE_{ST} = 0.30 eV, 0.23 eV, 0.22 eV
τ_d = 65 μs (10 wt% DPEPO), 135 μs, 158 μs (10 wt% PPT)
λ_{PL} = 482 nm (10 wt% DPEPO), 458 nm, 456 nm (10 wt% PPT)
Φ_{PL} = 69% (10 wt% DPEPO), 65%, 70% (10 wt% PPT)
$|g_{PL}| = 1.3\times10^{-3}$ (PhMe), n.a., n.a.
λ_{EL} = 480 nm, 456 nm, 460 nm
EQE_{max} = 17%, 7.4%, 12%
Chem. Sci. **2019**, *10*, 6689. *Mater. Adv.* **2021**, *2*, 6684.

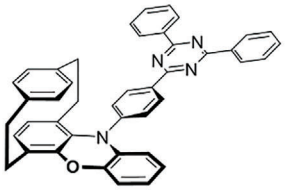

PXZp-Ph-TRZ
ΔE_{ST} = 0.03 eV
τ_d = 12 μs, (10 wt% CBP)
λ_{PL} = 548 nm (PhMe)
Φ_{PL} = 60% (neat)
$|g_{PL}| = 3.3\times10^{-3}$ (PhMe)
λ_{EL} = 560 nm, EQE_{max} = 7.8%, $|g_{EL}| = 4.6\times10^{-3}$
ACS Appl. Mater. Interfaces **2021**, *13*, 25186.

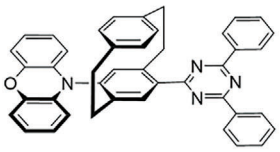

PXZ-PT
ΔE_{ST} = 0.19 eV
τ_d = 75 μs, (10 wt% CBP)
λ_{PL} = 565 nm (PhMe)
Φ_{PL} = 78% (10 wt% CBP)
$|g_{PL}| = 1.9\times10^{-3}$ (PhMe)
λ_{EL} = 557 nm, EQE_{max} = 20%, $|g_{EL}| = 1.5\times10^{-3}$
Mater. Horiz. **2021**, *8*, 3417.

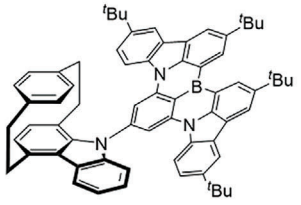

Czp-*t*BuCzB
ΔE_{ST} = 0.09 eV
τ_d = 42 μs (5 wt% 2,6DCzPPy)
λ_{PL} = 478 nm (PhMe)
Φ_{PL} = 98% (8 wt% 2,6DCzPPy)
$|g_{PL}| = 5.4\times10^{-4}$ (PhMe), 1.6×10^{-3} (2,6DCzPPy)
λ_{EL} = 479 nm, EQE_{max} = 32%, $|g_{EL}| = 1.5\times10^{-3}$

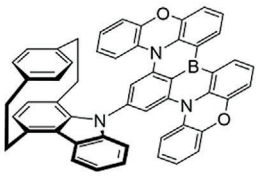

Czp-POAB
ΔE_{ST} = 0.13 eV
τ_d = 62 μs (8 wt% 2,6DCzPPy)
λ_{PL} = 498 nm (PhMe)
Φ_{PL} = 96% (8 wt% 2,6DCzPPy)
$|g_{PL}| = 4.8\times10^{-4}$ (PhMe), 1.4×10^{-3} (2,6DCzPPy)
λ_{EL} = 513 nm, EQE_{max} = 29%, $|g_{EL}| = 1.3\times10^{-3}$

Angew. Chem. Int. Ed. **2023**, *62*, e202217045.

This work

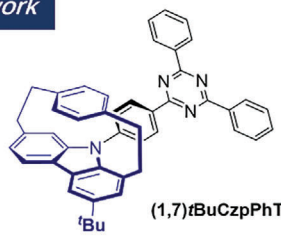

(1,7)*t*BuCzpPhTrz
ΔE_{ST} = 0.23 eV, τ_d = 637 μs (10 wt% DPEPO)
λ_{PL} = 473 nm and Φ_{PL} = 91% (10 wt% DPEPO)
$|g_{PL}| = 5\times10^{-4}$ (PhMe), λ_{EL} = 475 nm, EQE = 14%

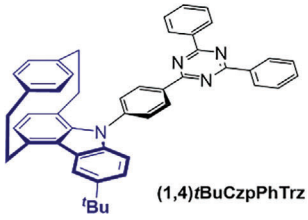

(1,4)*t*BuCzpPhTrz
ΔE_{ST} = 0.11 eV, τ_d = 315 μs (10 wt% DPEPO)
λ_{PL} = 480 nm and Φ_{PL} = 84% (10 wt% DPEPO)
$|g_{PL}| = 5\times10^{-4}$ (PhMe), λ_{EL} = 490 nm, EQE = 17%

Figure 1. Summary of reported [2.2]paracyclophane-based TADF Emitters.

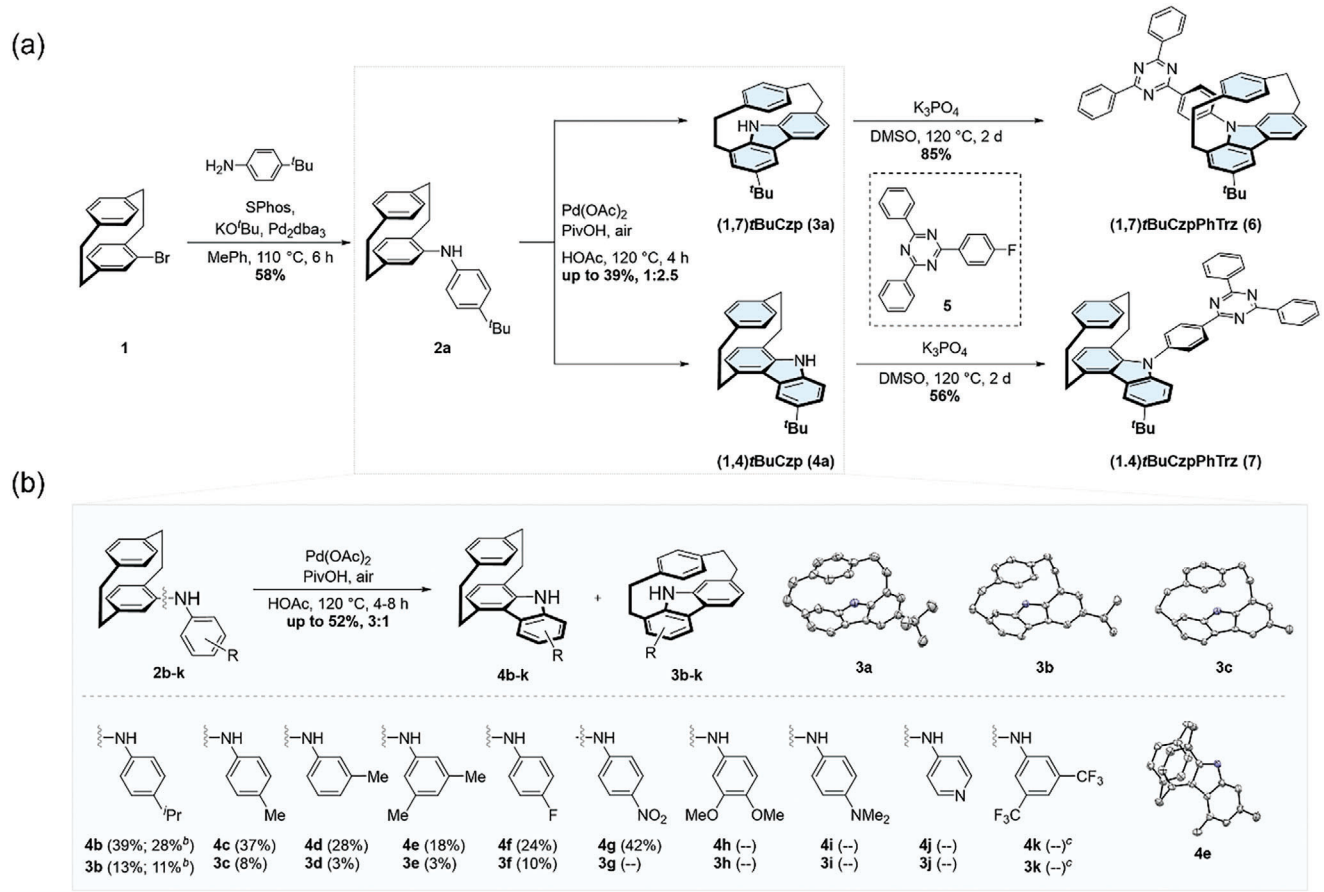

Scheme 1. a) Synthesis of emitters (*rac*)-(1,7)*t*BuCzpPhTrz and (*rac*)-(1,4)*t*BuCzpPhTrz. b) Synthetic scope of the oxidative cyclization of substituted phenylamino[2.2]paracyclophanes: 2 (3 mmol, 0.1 M), $Pd(OAc)_2$ (25 mol%), pivalic acid (75 mol%). Yields refer to isolated compounds. [a] 2a (25 mmol) was used. [b] $Pd(OAc)_2$ (20 mol%), pivalic acid (60 mol%) was used. [c] no conversion of 2k observed.

obtained by Pd-catalyzed oxidative cyclization of 4-*N*-(4-(*tert*-butyl)phenyl)amino[2.2]paracyclophane (**2a**) under aerobic conditions. In the presence of palladium(II) acetate and pivalic acid in acetic acid **(1,4)*t*BuCzp** and **(1,7)*t*BuCzp** were successfully formed in an overall yield of 39% in a ratio of 5:2. The latter implicates an unexpected migration of the ethylene bridge to the aniline arene, which was confirmed by X-ray diffraction analysis. In contrast to the planar geometry of the carbazole moiety in (1,4)Czp, an angle of 38° between the two benzene planes of the carbazole was measured in (1,7)carbazolophane (for more details see Figure S84, Supporting Information). On the basis of previous CH-activation studies,[19] we propose a mechanism for the oxidative cyclization/rearrangement sequence (Scheme S1, Supporting Information). For the initial *ortho* palladation step, we consider two intermediates, the relevant for **(1,7)*t*BuCzp** formation being **A** (Scheme S2, Supporting Information). Consecutive CH insertion of both *ortho* palladation states followed by reductive elimination affords the expected carbazolophane **(1,4)*t*BuCzp**. The alternative pathway from **A**, involves palladation of the distorted C(sp^2) bridgehead atom and a [1,5]-alkyl shift, which should result in a release of ring strain. Reductive elimination of palladacycle **C** and [1,3]-H shift provides **(1,7)*t*BuCzp** and reforms the active palladium catalyst. Such an alteration of the PCP skeleton through C—C bond breakage has rarely been documented in the literature.[20] Compared to the conventional route of photo-deselenation to afford mixed carbazolophanes,[21] this finding not only highlights an efficient alternative approach to synthesize this new class of carbazolophane derivatives, but also facilitates their use as building blocks of elaborated structures. For example, the amino group in **3** needs no protection and can serve as a reactive site for further functionalization.

In order to explore the compatibility of this protocol, we studied a series of phenylamino[2.2]paracyclophanes of varying electronic and steric demand. As shown in Scheme 1b, the reaction proceeded in good-to-moderate yields for *para*-alkylated substrates (**2a-c**) with an overall yield of up to 52% and a ratio of 1:3 for the methylated cyclophanes **3c** and **4c**, respectively. The reaction yields of the (1,4)Czp derivatives (**4b**, **4c**) are comparable to the previously reported studies; however, the formation of the (1,7)Czp derivatives (**3b**, **3c**) have not as of yet been documented.[18] A decrease in yield was observed for *meta*-substituted amines (**2d**, **2e**) due to the increase in steric hindrance. Consequently, only one selective regioisomer of **3d** and **4d** was formed. As determined by NMR spectroscopy analysis for both molecules, the carbazole C—C bond

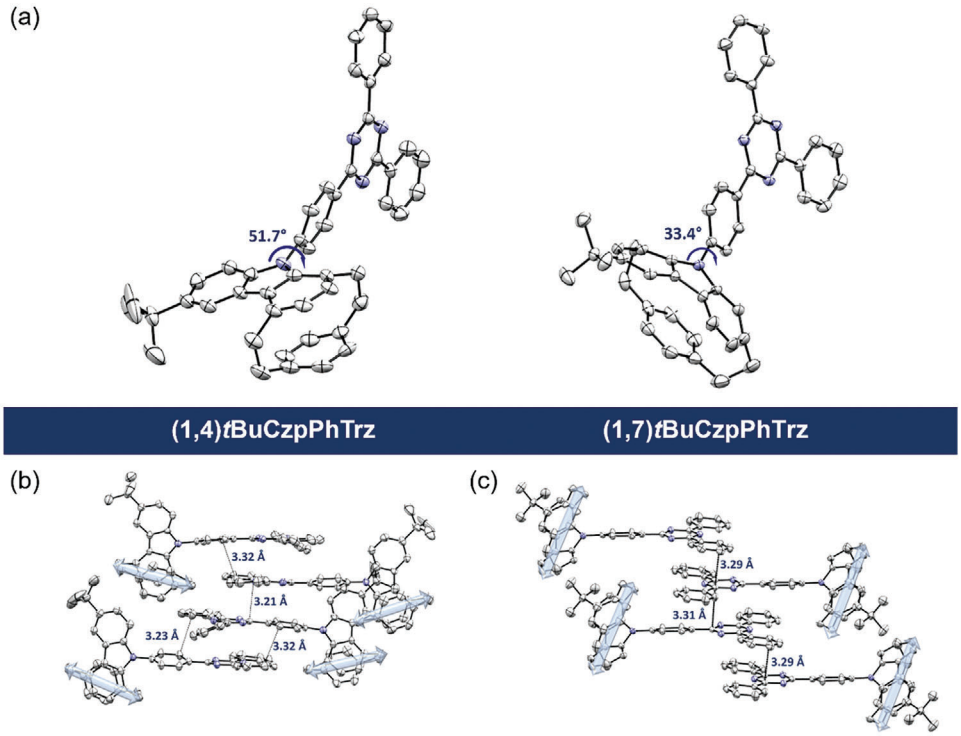

Figure 2. a) Molecular structures of (1,4)*t*BuCzpPhTrz (CCDC 2 305 740) and (1,7)*t*BuCzpPhTrz (CCDC 2 261 384). Displacement parameters are drawn at 50% probability level, hydrogen atoms are omitted for clarity. Schematic presentation of the π-π stacking along the triazine planes in b) (1,4)*t*BuCzpPhTrz and c) (1,7)*t*BuCzpPhTrz.

was formed at the less hindered position, confirming the observations of other Pd-catalyzed carbazole protocols based on CH-activation.[22] Electron-withdrawing groups in the *para* position are tolerated although slightly longer reaction times were required to achieve full conversion. No consumption was observed during the reaction of **2k**, bearing electron-deficient groups *meta* to the amine. However, oxidative cyclization of nitro-substituted **2g** yields solely the respective (1,4)carbazolophane **4g** in 42%. In general, highly reactive functionalities (**2h–j**) were found to be incompatible under the studied reaction conditions and led to decomposition.

To systematically explore the impact of these two cyclophane species in TADF materials, we selected **(1,7)*t*BuCzp** (**3a**) and **(1,4)*t*BuCzp** (**4a**) as examples to ensure high solubility of the donor-acceptor type molecules. The target materials **(1,7)*t*BuCzpPhTrz** (**6**) and **(1,4)*t*BuCzpPhTrz** (**7**) were prepared upon nucleophilic aromatic substitution with 2-(4-fluorophenyl)−4,6-diphenyl-1,3,5-triazine (**5**) and isolated in 85 and 56% yield, respectively. The two emitters were fully characterized by nuclear magnetic resonance (NMR) spectroscopy, infrared (IR) spectroscopy, melting point analysis (Mp), high resolution mass spectrometry (HRMS), high performance liquid chromatography (HPLC), and elemental analysis (EA) (details see ESI). Single crystals suitable for X-ray diffractometry were collected during sublimation or by slow evaporation from *n*-hexane/CH_2Cl_2 solution and unambiguously confirmed the molecular structure of both target materials (**Figure 2**). For the following photophysical and optoelectronic characterization, the emitters were used in their racemic form. The chiroptical properties were studied with the resolved starting materials (R_p)/(S_p)-**(1,4)*t*BuCzp** and (R_p)/(S_p)-**(1,7)*t*BuCzp**, which were isolated by semi-preparative HPLC on a chiral stationary phase in high enantiomeric excess (ee) of >98% for each. Subsequent conversion yielded (R_p)/(S_p)-**(1,4)*t*BuCzpPhTrz** and (R_p)/(S_p)-**(1,7)*t*BuCzpPhTrz** in a purity of >99/98% *ee* and >92/98% *ee*, respectively (Scheme S3).

Crystallographic analysis revealed that the carbazole of **(1,4)*t*BuCzpPhTrz** engages in π-stacking with the cyclophane deck in an analogous manner to the parent emitter, **(1,4)CzpPhTrz (aka CzpPhTrz)**, previously reported by us.[12b] The carbazole moiety of **(1,7)*t*BuCzpPhTrz** adopts a puckered conformation and the ethylene C–C bonds of the PCP are much shorter than those in **(1,4)*t*BuCzpPhTrz** (1.56 Å vs 1.58 Å). This brings the carbazole and phenylene rings closer together (2.31–3.33 Å) than in **(1,4)*t*BuCzpPhTrz** (2.76–3.09 Å). Due to the spatial orientation of the ethylene bridges in **(1,7)*t*BuCzpPhTrz**, which are positioned perpendicular to the triazine axis, the torsion angle between the pyrrole core of the carbazole to the grafted phenylene of the triazine in **(1,7)*t*BuCzpPhTrz** is shallower (33.4°) compared to **(1,4)*t*BuCzpPhTrz** (51.7°) and **(1,4)CzpPhTrz** (51.8°), where the steric hindrance of the cyclophane bridge becomes more pronounced. The compounds pack through π-π stacking of the triazine moieties, with the neighboring triazines facing towards each other in an anti-parallel fashion (Figure 2b,c). The intermolecular distance of these π-π stacked planes in the two crystal structures of the two compounds is in a similar range of around 3.3 Å.

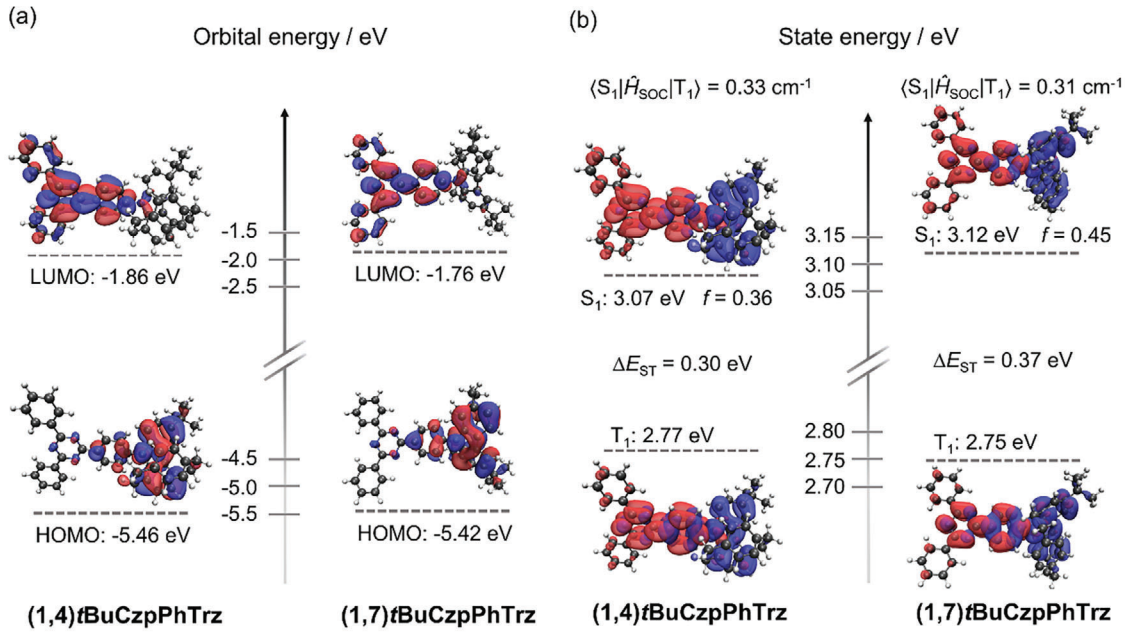

Figure 3. Theoretical modeling of a) the energies and electron density distributions of the HOMO/LUMO (ISO value = 0.02) and b) NTOs (particle and hole are represented by red and blue colors, respectively) and their associated vertical excitation energies of S_1 and T_1 states of (1,4)*t*BuCzpPhTrz and (1,7)*t*BuCzpPhTrz computed based on the ground-state optimized geometries, *f* is the oscillator strength.

2.2. Theoretical Calculations

We undertook a theoretical study to understand the impact of the connectivity of the cyclophane on the optoelectronics of the emitters. The ground-state optoelectronic properties of **(1,4)*t*BuCzpPhTrz** and **(1,7)*t*BuCzpPhTrz** were calculated using density functional theory (DFT) at the PBE0/6-31G(d,p) level in the gas phase. As shown in **Figure 3**, the torsion angles between the donor and acceptor moieties are around 55.5° for **(1,4)*t*BuCzpPhTrz** and 36.2° for **(1,7)*t*BuCzpPhTrz**, which are in agreement to the angles found in the crystal structures (51.7° and 33.4°, respectively). The HOMO is mainly localized on the **(1,4)*t*BuCzp** or **(1,7)*t*BuCzp** donors with a small degree of electron density on the bridging phenylene, the HOMO energy levels are nearly identical at −5.46 and −5.42 eV, respectively. Similarly, the lowest unoccupied molecular orbital (LUMO) is located on the triazine acceptor and the bridge, with the LUMO of **(1,7)*t*BuCzpPhTrz** being slightly destabilized at −1.76 eV compared to that of **(1,4)*t*BuCzpPhTrz** at −1.86 eV. The HOMO-LUMO gap is thus essentially the same in the two compounds.

Time-dependent DFT (TD-DFT) calculations within the Tamm-Dancoff approximation (TDA-DFT), performed at the same level of theory, predict that both compounds have large ΔE_{ST} of 0.30 and 0.37 eV for **(1,4)*t*BuCzpPhTrz** and **(1,7)*t*BuCzpPhTrz**, respectively. Both compounds have similar predicted S_1 levels to the parent **(1,4)CzpPhTrz** (S_1 level of 3.11 eV) and the S_1 state is predicted to show CT character with a high oscillator strength for the S_0-S_1 transition. However, their triplet levels are more stabilized compared to the T_1 of **(1,4)CzpPhTrz** (2.81 eV), with predicted T_1 levels of 2.77 and 2.75 eV for **(1,4)*t*BuCzpPhTrz** and **(1,7)*t*BuCzpPhTrz**. There is a large spin-orbital coupling constant between the S_1 and T_1 states at their optimized ground-state geometries (0.33 cm^{-1} for **(1,4)*t*BuCzpPhTrz** and 0.31 cm^{-1} for **(1,7)*t*BuCzpPhTrz**). The NTO analysis of both compounds based on the optimized S_1 and T_1 geometries were also calculated (Figure S100, Supporting Information). For both compounds the S_1 and T_1 states showed similar location of particles mainly on the triazine group and holes mainly on the donor groups, indicating that both states possess CT character. Thus, on balance and despite the large predicted ΔE_{ST} values, these two compounds are predicted to show TADF and emit in the blue.

2.3. Electrochemistry

The energies of the HOMO and LUMO were inferred from cyclic voltammetry (CV) and differential pulse voltammetry (DPV) measurements in deaerated dichloromethane containing 0.1 M $[^nBu_4N]PF_6$ as the supporting electrolyte (Figure S101, Supporting Information). The electrochemical data are summarized in **Table 1**. The E_{ox}/E_{red} values, determined from the DPV peaks, are 1.08 V/−1.72 V and 1.13 V/−1.74 V for **(1,4)*t*BuCzpPhTrz** and **(1,7)*t*BuCzpPhTrz**, respectively, versus SCE, with corresponding HOMO/LUMO values of −5.42 eV/−2.62 eV and −5.47 eV/−2.60 eV. The redox gaps of 2.80 V and 2.87 V for **(1,4)*t*BuCzpPhTrz** and **(1,7)*t*BuCzpPhTrz** largely mirror the calculated HOMO-LUMO gaps.

2.4. Photophysical Measurements

We next measured the photophysical properties of the two compounds in dilute (10^{-5} M) toluene solution at 298 K (**Figure 4a**

Table 1. Summary of CV and DPV results.

	E_{ox} [a] [V] vs SCE	E_{red} [a] [V] vs SCE	HOMO [b] [eV]	LUMO [b] [eV]	ΔE_{redox} [c] [V]
(1,4)*t*BuCzpPhTrz	1.08	−1.72	−5.42	−2.62	2.80
(1,7)*t*BuCzpPhTrz	1.13	−1.74	−5.47	−2.60	2.87

[a] measured in N_2-saturated DCM (0.46 V for DCM versus SCE[23]) with a scan rate of 0.1 V/s; [b] HOMO and LUMO energies were determined using $E_{HOMO/LUMO} = -(E_{ox}/E_{red}+4.8)$ eV[24] where E_{ox} and E_{red} are determined from the peak of the DPVs, respectively, versus Fc/Fc^+; [c] $\Delta E_{redox} = |E_{ox}\text{-}E_{red}|$.

and **Table 2**). The absorption spectra for both compounds have intense bands at around 385 nm, which are assigned by TDA-DFT calculations to the intramolecular charge transfer between the donor and the triazine acceptor. This assignment is also in line with that for **(1,4)CzpPhTrz** which has an ICT absorption band at 375 nm. The ICT band of **(1,7)*t*BuCzpPhTrz** has a higher molar absorptivity value ($\varepsilon = 45 \times 10^3$ M^{-1} cm^{-1}) than **(1,4)*t*BuCzpPhTrz** ($\varepsilon = 29 \times 10^3$ M^{-1} cm^{-1}), indicating a higher oscillator strength for the S_0 and S_1 transition, which is in line with the trend in predicted S_1 oscillator strengths. The steady-state photoluminescence (PL) spectra in toluene are broad and unstructured, as typically observed in donor-acceptor TADF compounds, with peak maxima, λ_{PL}, at 466 and 446 nm for **(1,4)*t*BuCzpPhTrz** and **(1,7)*t*BuCzpPhTrz**, respectively. Notably, the full width at half maxima (FWHMs) are different at 76 and 50 nm, respectively, suggesting that there is less geometric reorganization in the excited state of **(1,7)*t*BuCzpPhTrz** than **(1,4)*t*BuCzpPhTrz**. The emission of both compounds is blue-shifted compared to that of **(1,4)CzpPhTrz** (λ_{PL} of 470 nm in toluene). There is an observed positive solvatochromism in the PL of both compounds (Figure S102, Supporting Information), which corroborates the assignment of the S_1 state as having CT character. The optical gap (E_g), determined from the intersection of the normalized absorption and emission spectra, are 2.94 eV and 2.99 eV for **(1,4)*t*BuCzpPhTrz** and **(1,7)*t*BuCzpPhTrz**, respectively. The Φ_{PL} values of **(1,4)*t*BuCzpPhTrz** and **(1,7)*t*BuCzpPhTrz** in degassed toluene solutions are 82 and 78%, respectively, which decrease to 68 and 72% upon exposure to oxygen. The time-resolved emission decays for both compounds have lifetimes, τ_{PL}, of 8.2 and 4.2 ns, no obvious delayed emission was detected.

We next investigated their photophysical properties in both a wide bandgap polymer host, PMMA, and also a high triplet energy small molecule host, DPEPO (T_1 = 3 eV[25]), with a view to employing these compounds as emitters in OLEDs. The concentration of the doped films was chosen as 10 wt% as this is what was used for the previous study with **(1,4)CzpPhTrz**. **(1,4)*t*BuCzpPhTrz** and **(1,7)*t*BuCzpPhTrz** showed unstructured CT-based emission at λ_{PL} of 470 and 457 nm as in 10 wt% doped films in PMMA, respectively (Figure 4b). The FWHMs are 83 and 66 nm, respectively, which are slightly broader than FWHMs measured in toluene of 76 and 50 nm. These emission spectra are red-shifted to 480 and 473 nm in 10 wt% doped films in DPEPO, with FWHMs of 87 and 69 nm, reflecting the higher polarity of this host compared to PMMA. These λ_{PL} values are similar to that reported for **(1,4)CzpPhTrz** (λ_{PL} = 482 nm in 10 wt% doped films in DPEPO). The Φ_{PL} values of the doped DPEPO films of **(1,4)*t*BuCzpPhTrz** and **(1,7)*t*BuCzpPhTrz** are 84 and 91%, respectively, which decrease to 78 and 81% under air, respectively. The Φ_{PL} values in 10 wt% doped films of **(1,7)*t*BuCzpPhTrz** in DPEPO are similar to those of the 10 wt% doped films in mCP:PPT (1:1); the λ_{PL} values of 473 and 463 nm in doped mCP:PPT (1:1) films mirror those in PMMA (Table S9, Supporting Information). In 10 wt% doped films in mCP:PPT, the Φ_{PL} of **(1,4)*t*BuCzpPhTrz** is slightly lower at 77% under N_2 and 68% under air.

The S_1 and T_1 energies for both compounds were extracted from the onsets of the steady-state PL and delayed emission spectra (1–10 ms) at 77 K in both 2-MeTHF glass and the 10 wt% doped films in DPEPO (**Figure 5**). The ΔE_{ST} values of **(1,4)*t*BuCzpPhTrz** and **(1,7)*t*BuCzpPhTrz** are 0.11 and 0.23 eV in 2-MeTHF, while those in 10 wt% doped films in DPEPO are 0.18 and 0.25 eV, respectively. These are smaller than the calculated ΔE_{ST} values and reflect the impact of the host in modulating the energies of the excited states. The larger ΔE_{ST} for **(1,7)*t*BuCzpPhTrz** results from the smaller D-A torsion angle,

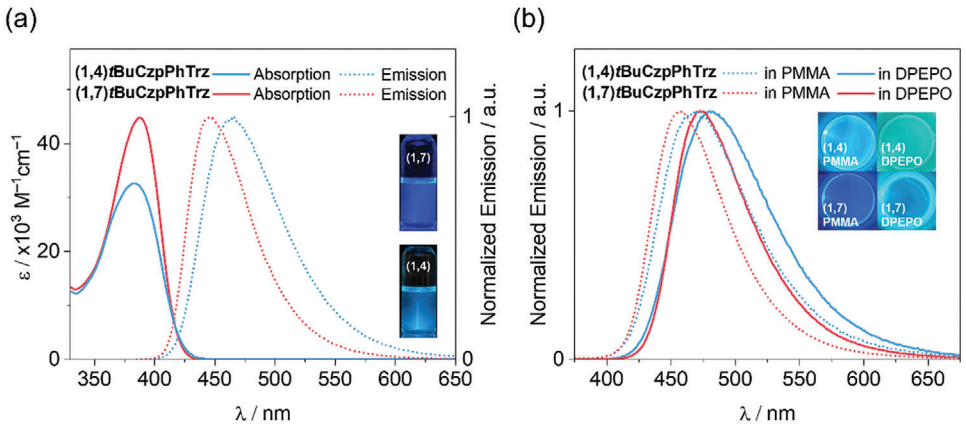

Figure 4. a) UV–vis absorption and PL spectra of (1,4)*t*BuCzpPhTrz (blue) and (1,7)*t*BuCzpPhTrz (red) in 10^{-5} M toluene solution (λ_{exc} = 365 nm). b) PL spectra (λ_{exc} = 360 nm) in 10 wt% doped films.

Table 2. Photophysical properties of (1,4)*t*BuCzpPhTrz and (1,7)*t*BuCzpPhTrz.

Compound	λ_{abs} [a] [nm]	λ_{PL} [a] [nm]	λ_{PL} [b] [nm]	Φ_{PL} [a] [%]	Φ_{PL} [b] [%]	E_g [c] [eV]	τ_p [a,d] [ns]	τ_p [b,d] [ns]	τ_d [b,d] [µs]	S_1/T_1 [e] [eV]	ΔE_{ST} [e] [eV]
(1,4)*t*BuCzpPhTrz	384	466	480	82(68)	84(78)	2.94	8.2	8.9	315	2.97/2.79	0.11
(1,7)*t*BuCzpPhTrz	388	446	473	78(72)	91(81)	2.99	4.2	5.3	637	2.92/2.72	0.23

[a] In toluene at 298 K; [b] Thin films were prepared by vacuum depositing at 10 wt% doping in DPEPO (λ_{exc} = 360 nm); [c] The optical bandgaps were calculated from the intersection point of the normalized absorption and emission spectra; [d] Average lifetime ($\tau_{avg} = \Sigma A_i\tau_i^2/\Sigma A_i\tau_i^2$, where A_i is the preexponential for lifetime τ_d). Prompt and delayed emissions were measured by TCSPC and MCS, respectively (λ_{exc} = 379 nm); [e] Determined from the onset of prompt and delayed spectra in 2-MeTHF, measured at 77 K.

as determined in the crystal structure analysis, that leads to a larger exchange integral. The time-resolved PL decays of the 10 wt% doped films of **(1,4)*t*BuCzpPhTrz** and **(1,7)*t*BuCzpPhTrz** in DPEPO at room temperature show a prompt fluorescence lifetime, τ_p, of 8.9 and 5.3 ns, and an average delayed fluorescence lifetime, τ_d, of 315 and 637 µs, respectively (**Figure 6**a,b). The delayed emission is significantly quenched in the presence of oxygen while the prompt emission is invariant. The temperature-dependent time-resolved PL decays (Figure 6c,d) reveal the expected increase in the intensity of the delayed emission with increasing temperature that is emblematic of TADF.

2.5. Chiroptical Properties

We next measured the chiroptical properties of both enantiomeric pairs. The electronic circular dichroism (ECD) spectra of both compound pairs display mirror image behavior in tetrahydrofuran (**Figure 7**). A pronounced band is observed for **(1,4)*t*BuCzpPhTrz** at 219 nm ($\Delta\varepsilon$ = +77.8 M^{-1} cm^{-1} for R_p), while weaker responses are found at 261 nm ($\Delta\varepsilon$ = −11 M^{-1} cm^{-1} for R_p), 280 nm ($\Delta\varepsilon$ = +16 M^{-1} cm^{-1} for R_p) and 308 nm ($\Delta\varepsilon$ = +78 $M^{-1}cm^{-1}$ for R_p). The CT absorption band at 380 nm ($\Delta\varepsilon$ = −8.4 M^{-1} cm^{-1} for R_p) is of similar wavelength to that reported for other (1,4)carbazolophane-based compounds.[12b,16] An

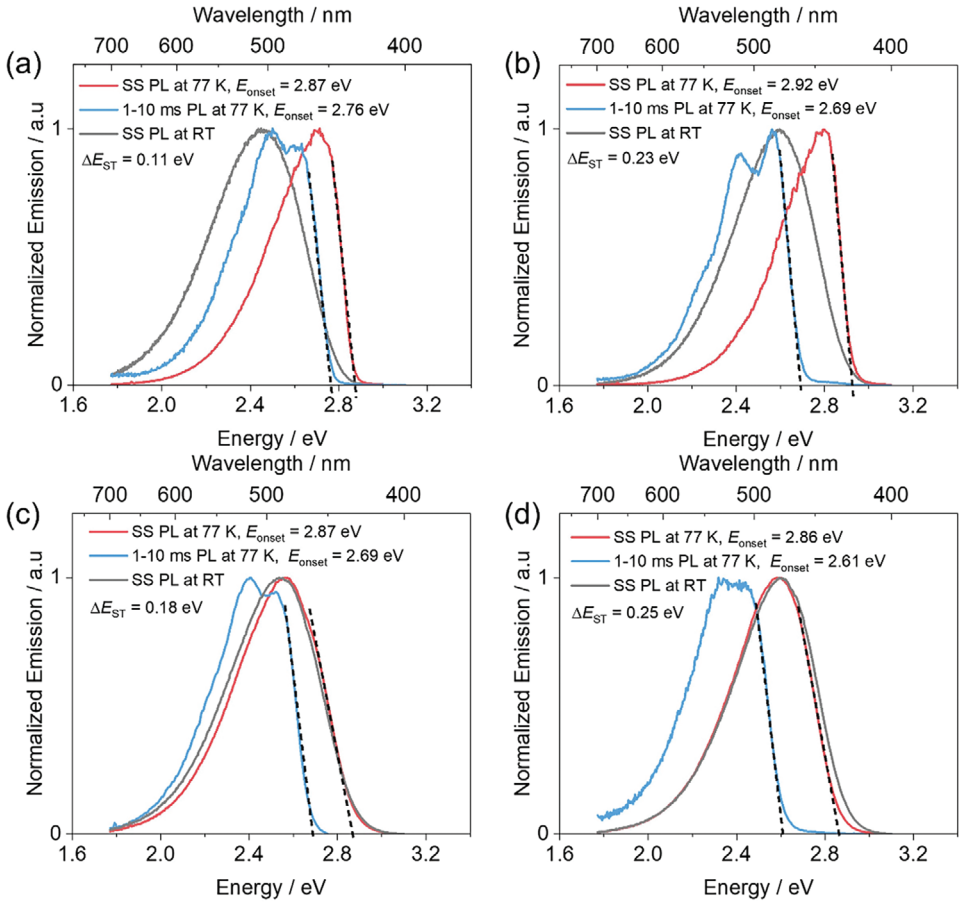

Figure 5. Steady-state PL at RT and 77 K and time-gated emission (1–10 ms) spectra at 77 K. a) (1,4)*t*BuCzpPhTrz in 2-MeTHF glass (λ_{exc} = 375 nm). b) (1,7)*t*BuCzpPhTrz in 2-MeTHF glass (λ_{exc} = 375 nm). c) (1,4)*t*BuCzpPhTrz as a 10 wt% doped films in DPEPO (λ_{exc} = 375 nm). d) (1,7)*t*BuCzpPhTrz as a 10 wt% doped films in DPEPO (λ_{exc} = 365 nm).

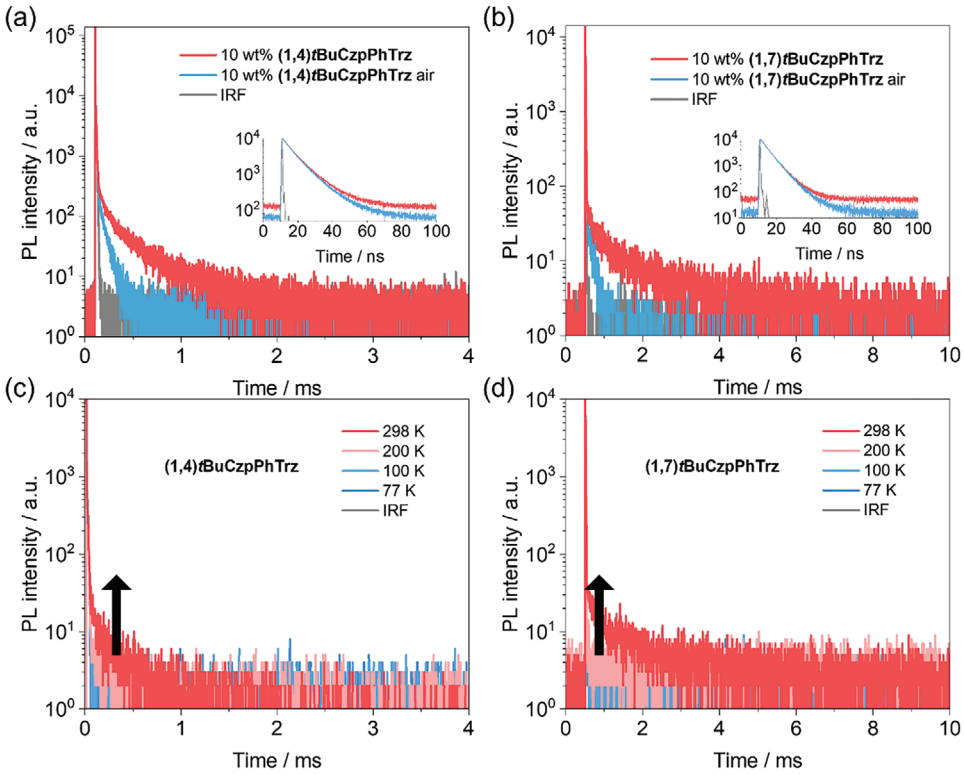

Figure 6. Time-resolved PL decay within millisecond and 100 ns time windows (inset) of 10 wt% doped films in DPEPO in air and under vacuum of a) (1,4)*t*BuCzpPhTrz (λ_{exc} = 375 nm) and b) (1,7)*t*BuCzpPhTrz (λ_{exc} = 375 nm). Temperature-dependent time-resolved PL decays of 10 wt% doped films in DPEPO of c) (1,4)*t*BuCzpPhTrz (λ_{exc} = 375 nm) and d) (1,7)*t*BuCzpPhTrz (λ_{exc} = 375 nm). IRF = instrument response function.

absorption dissymmetry factor (g_{abs}) of -6×10^{-4} at 380 nm was determined for (R_p)-**(1,4)*t*BuCzpPhTrz**. For **(1,7)*t*BuCzpPhTrz**, three main bands are observed at 261 nm ($\Delta\varepsilon = +16$ M^{-1} cm^{-1} for R_p), 314 nm ($\Delta\varepsilon = +15$ M^{-1} cm^{-1} for R_p) and the CT band at 388 nm ($\Delta\varepsilon = -6.2$ M^{-1} cm^{-1} for R_p). The g_{abs} of -4×10^{-4} at 388 nm for (R_p)-**(1,7)*t*BuCzpPhTrz** was found to be in the same order than the (1,4) isomer. The absolute configurations of the enantiomers were determined by comparison of the experimental data with predicted spectra based on TD-DFT calculations at the M06/6-311++G(d,p) level with an implicit solvent field using the conductor-polarized continuum model (CPCM).[26] The second enantiomer of **(1,4)*t*BuCzp** was assigned to be (S_p), while for **(1,7)*t*BuCzp** the first isolated enantiomer was assigned to be (R_p) (Figure S85, Supporting Information). The ECD spectra of the derived emitters (S_p)-**(1,4)*t*BuCzpPhTrz** and (R_p)-**(1,7)*t*BuCzpPhTrz** broadly match the predicted spectra (Figure 7a,b). The circularly polarized luminescence (CPL) spectra of both emitters in toluene displayed mirror-image and unstructured CPL in the region between 425 to 600 nm (λ_{exc} = 350 nm) with peaks observed at 465 nm for (R_p)/(S_p)-**(1,4)*t*BuCzpPhTrz** and 447 nm for (R_p)/(S_p)-**(1,7)*t*BuCzpPhTrz** (Figure 7c,d). The corresponding g_{PL} values are -5×10^{-4} with negative signals for the (R_p) enantiomers. Interestingly, as shown in Figure S99 (Supporting Information), the g_{PL} spectra are constant throughout the whole emission band, affording further evidence of the nearly pure CT character of the emission for these chiral systems. Furthermore, the g_{PL}/g_{abs} ratios of +0.8 and +1.25 for **(1,4)*t*BuCzpPhTrz** and **(1,7)*t*BuCzpPhTrz**, respectively, also indicate weak structural/electronic reorganization during excitation/emission processes. These dissymmetry factors are comparable to those of PCP-based compounds,[3b] suggesting that the incorporation of cyclophanyl-based planar chirality is a promising strategy for generating CPL-active emitters.

2.6. Organic Light-Emitting Diodes

Having identified the potential of these compounds as emitters, vacuum-deposited OLEDs with **(1,4)*t*BuCzpPhTrz** and **(1,7)*t*BuCzpPhTrz** were fabricated. The first set of OLEDs was made using our previously reported stack,[12b] with DPEPO as the host. **Figure** 8a,b shows the schematic of the device layout and the chemical structures of the organic materials. The device structure was: indium tin oxide (ITO)/N,N-di(1-naphthyl)-N,N-diphenyl-(1,1-biphenyl)−4,4-diamine (NPB, 30 nm)/tris(4-carbazoyl-9-ylphenyl)amine (TCTA, 20 nm)/mCP (10 nm)/DPEPO (20 nm) with 10 wt% of **(1,4)*t*BuCzpPhTrz** or **(1,7)*t*BuCzpPhTrz**/DPEPO (10 nm)/1,3,5-tris(3-pyridyl-3-phenyl)benzene (TmPyPB, 40 nm)/lithium fluoride (LiF, 0.8 nm)/aluminum (Al, 100 nm). Here, NPB, TCTA and mCP served as hole injection, transport, and exciton blocking layers, respectively, while TmPyPB and DPEPO were used as electron transport, and hole blocking layers, respectively. The comparison of current density-voltage-luminance (JVL) characteristics for both devices is shown in Figure 8c. The devices with (1,4)*t*BuCzpPhTrz and (1,7)*t*BuCzpPhTrz using DPEPO as the

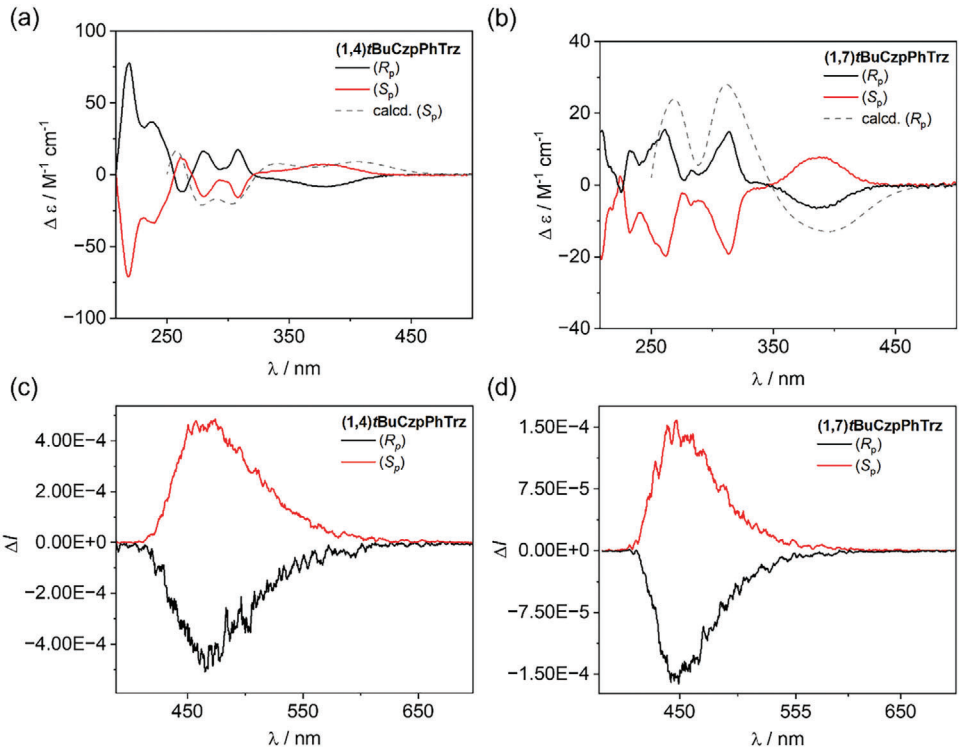

Figure 7. Experimental and calculated ECD spectra of a) $(R_p)/(S_p)$-(1,4)*t*BuCzpPhTrz and b) $(R_p)/(S_p)$-(1,7)*t*BuCzpPhTrz measured in tetrahydrofuran. Predicted spectra were calculated at the TD-DFT-M06/6-311++G(d,p) with an implicit tetrahydrofuran solvent field (cpcm). CPL spectra of c) $(R_p)/(S_p)$-(1,4)*t*BuCzpPhTrz and d) $(R_p)/(S_p)$-(1,7)*t*BuCzpPhTrz in toluene (λ_{exc} = 350 nm).

host had high turn-on voltages of 3.7 and 4.3 V, respectively. This indicated that DPEPO was not a favorable host, likely causing charge trapping on the host or charge accumulation at the EML interfaces.[27] Even though the devices with **(1,4)*t*BuCzpPhTrz** (Figure 8d) showed an EQE_{max} of 18.5%, the efficiency roll-off was severe as the EQE_{100} (EQE at 100 cd m^{-2}) was 8% while the EQE_{1000} (EQE at 1000 cd m^{-2}) decreased to 2.2%. The previously-reported device with **(1,4)CzpPhTrz** showed an EQE_{max} of 17% and a slightly improved efficiency roll-off, with the EQE_{100} of 12%.[12b] The more pronounced efficiency roll-off in the devices with **(1,4)tBuCzpPhTrz** as compared to the reported device with **(1,4)CzpPhTrz** may in part be due to the longer t_d (315 µs) of the former as compared to the t_d (65 µs) of the latter. Emitters with longer t_d typically correlate with devices showing more severe efficiency roll-off.[28] The device with **(1,7)*t*BuCzpPhTrz** achieved a comparable EQE_{max} of 18%, but the efficiency roll-off was even more pronounced with the EQE_{100}/EQE_{1000} dropping to 4.8/1.1%. The electroluminescence (EL) spectra for these two devices were similar with emission peaks, λ_{EL}, at 486 and 490 nm for the devices with **(1,4)*t*BuCzpPhTrz** and **(1,7)*t*BuCzpPhTrz**, respectively (Figure 8e). The CIE coordinates for devices with both emitters were also similar at (0.19, 0.33) (Figure 8f).

In an effort to reduce the efficiency roll-off, a second set of devices was fabricated using a 1:1 mixture of mCP and PPT. The use of this ambipolar co-host system was expected to result in a wider recombination zone and improve the mobility of both charges. The device structure (Figure 8a) was thus modified to be: ITO/1,4,5,8,9,11-hexaazatriphenylenehexacarbonitrile (HATCN, 10 nm)/1,1-bis[(di-4-tolylamino)phenyl]cyclohexane (TAPC, 25 nm)/TCTA (10 nm)/mCP (10 nm)/mCP:PPT (20 nm) with 10 wt% of **(1,4)*t*BuCzpPhTrz** or **(1,7)*t*BuCzpPhTrz**/PPT (10 nm)/TmPyPB (40 nm)/LiF (0.8 nm)/Al (100 nm). The thickness of the layers was optimized based on simulations for out-coupling efficiencies, and layer thicknesses were varied in increments of 5 nm to identify the best combination of optical and electrical properties (Figure S103, Supporting Information). Here, HATCN was used as the hole injection layer, TAPC as the hole transport layer, TCTA as electron blocking, mCP as the exciton blocking layer, PPT as the hole blocking layer, and TmPyPB for electron injection and transport.

The turn-on voltages were lower at 3.1 and 3.0 V for the devices with **(1,4)*t*BuCzpPhTrz** and **(1,7)*t*BuCzpPhTrz**, respectively, compared to those using DPEPO, indicating that the co-host system improved charge injection into the EML. This was also reflected in the higher current density and luminance as compared to the devices with DPEPO (Figure 8c). The EQE_{max} of the OLEDs with **(1,4)*t*BuCzpPhTrz** decreased slightly to 17%, but there was a modest improvement in the efficiency roll-off where the EQE_{100}/EQE_{1000} were maintained at 11.2/4.8%. Similarly, the device with **(1,7)*t*BuCzpPhTrz** showed a lower EQE_{max} of 13.5%; however, the EQE_{1000} (3.2%) was slightly improved compared to the device using DPEPO. One factor that may contribute to the higher EQE for the device with **(1,4)*t*BuCzpPhTrz** compared to that with **(1,7)*t*BuCzpPhTrz** is the greater horizontal orientation of the transition dipole moment of the emitter in the former (Figure S104, Supporting Information). The λ_{EL} for the

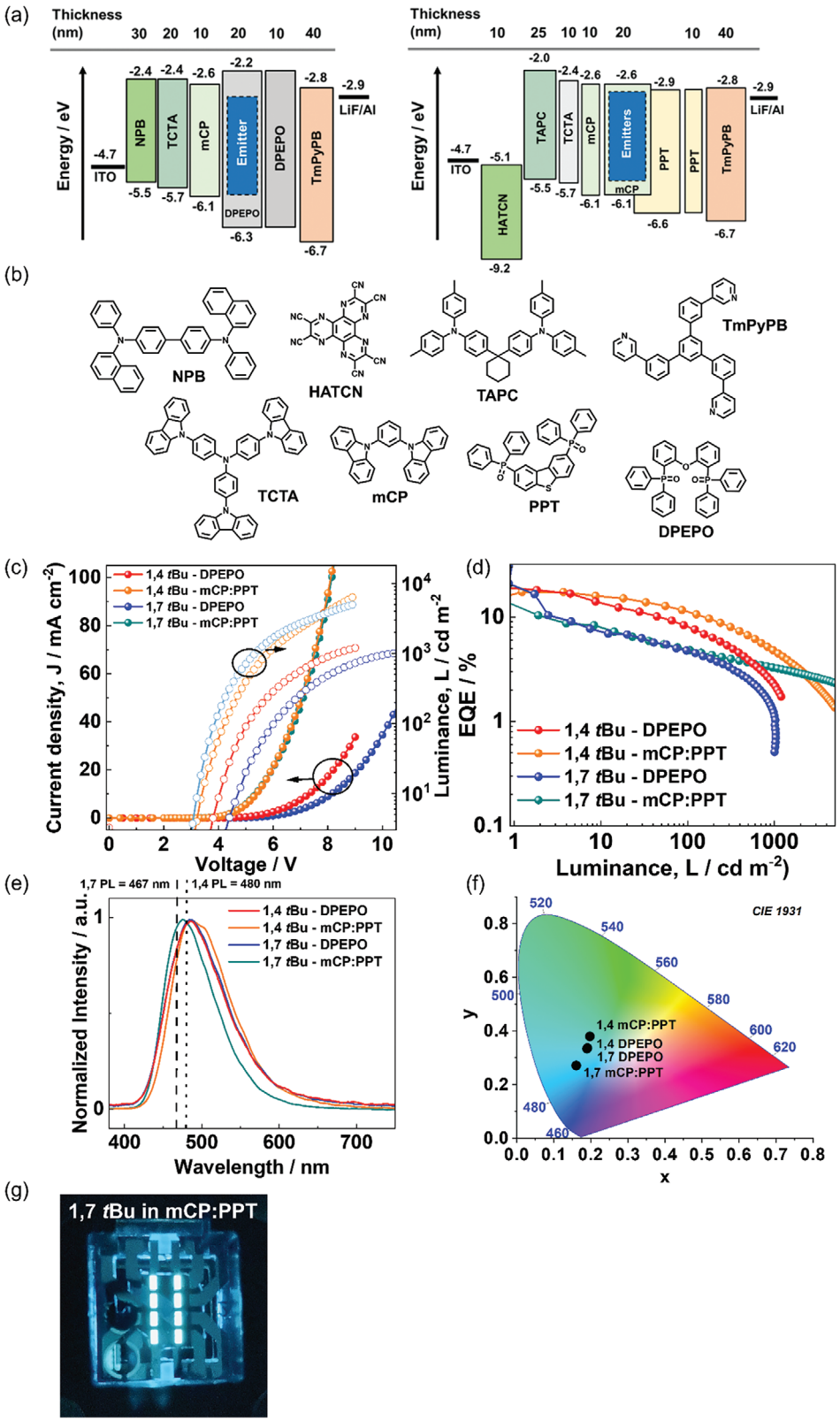

Figure 8. a) Schematic of the OLED device structures. b) Chemical structures of the organic materials used in the devices. c) Current density-Voltage-Luminance (JVL) curves. d) External quantum efficiency (EQE) versus Luminance. e) Electroluminescence spectra from the fabricated devices. f) CIE coordinates of the devices with (1,4)tBuCzpPhTrz and (1,7)tBuCzpPhTrz using either DPEPO or 1:1 mCP:PPT as hosts. g) Photograph of the OLEDs with (1,7)tBuCzpPhTrz in 1:1 mCP:PPT.

device with **(1,4)*t*BuCzpPhTrz** was 490 nm, which was similar to that of the device using DPEPO (486 nm). The λ_{EL} for the device with **(1,7)*t*BuCzpPhTrz** was 475 nm, which was blue-shifted compared to the device using DPEPO (490 nm), but is close to the λ_{PL} (467 nm in 1:1 mCP:PPT). These results point to a reduced propensity to aggregate in the co-host system compared to DPEPO for the vacuum-deposited films with **(1,7)*t*BuCzpPhTrz**. Indeed, aggregates were found to contribute to a red-shifting of the emission of **(1,7)*t*BuCzpPhTrz** in the 1:1 mCP:PPT co-host only at higher doping concentrations (Figure S105, Supporting Information). The CIE coordinates for the device with **(1,4)*t*BuCzpPhTrz** were (0.19, 0.38) while those for the device with **(1,7)*t*BuCzpPhTrz** were (0.16, 0.27) (Figure 8f,g) shows the photograph of the (1,7)tBuCzpPhTrz OLED in mCP:PPT cohost.

3. Conclusion

Here, we disclosed a new design concept to introduce planar chirality into TADF emitters by employing a novel cyclophane ([2]paracyclo[2]-3-*tert*butyl(1,7)carbazolophane, (1,7)*t*BuCzp) as a donor unit. This building block is obtained through an oxidative cyclization method involving an atypical rearrangement process. Due to its puckered geometry, carbazolophane **(1,7)*t*BuCzp** is a weaker donor than **(1,4)*t*BuCzp**. Photophysical studies showed a sharper, slightly blue-shifted emission of **(1,7)*t*BuCzpPhTrz** with a λ_{PL} of 446 nm and FWHM of 50 nm compared to **(1,4)*t*BuCzpPhTrz** (λ_{PL} = 466 nm, FWHM = 76 nm). The TADF character of both compounds was verified, **(1,7)*t*BuCzpPhTrz** has a superior Φ_{PL} of 91% (λ_{PL} = 473 nm) versus 84% (λ_{PL} = 480 nm) for **(1,4)*t*BuCzpPhTrz**. The enantiomeric pairs exhibited mirror image CPL behavior with $|g_{PL}|$ of 5×10^{-4}. Blue OLEDs with **(1,4)*t*BuCzpPhTrz** and **(1,7)*t*BuCzpPhTrz** achieved comparable $EQE_{max.}$ values of 19 and 18%, respectively. The initial devices were found to suffer from high-efficiency roll-off, which was improved by changing the host from DPEPO to a 1:1 mCP:PPT co-host system. This led to an $EQE_{max.}$ of 17% for the device with **(1,4)*t*BuCzpPhTrz** and a lower EQE_{max} of 14% for the **(1,7)*t*BuCzpPhTrz** device. The efficiency roll-off at high luminance (100 to 1000 cd m^{-2}) was alleviated from 73% to 57% for the OLED with **(1,4)*t*BuCzpPhTrz** and from 77% to 35% for the OLED with **(1,7)*t*BuCzpPhTrz**. We believe that this report provides fundamental insights for the development of planar chiral TADF materials and the impact of the cyclophane structure to achieve narrower emission.

Supporting Information

Supporting Information is available from the Wiley Online Library or from the author.

Acknowledgements

J.S., Y.X. and H.H. contributed equally to this work. The authors gratefully acknowledge the support provided by the Jürgen Manchot Foundation, the Karlsruhe School of Optics and Photonics and the Helmholtz Association Program at the Karlsruhe Institute of Technology. The authors further acknowledge the support by the state of Baden-Württemberg through bwHPC and funding by the Deutsche Forschungsgemeinschaft (DFG, German Research Foundation) under Germany's Excellence Strategy for the Excellence Cluster "3D Matter Made to Order" (EXC-2082/1–390761711). The authors would also like to express thanks to Dr. Erik Strandberg and Bianca Posselt, for their help in ECD measurements. The authors thank the China Scholarship Council (202 106 310 038), EPSRC (grants EP/R035164/1, EP/W015137/1, and EP/W524505/1) for financial support and acknowledge the Ministère de l'Enseignement Supérieur et de la Recherche and the Centre National de la Recherche Scientifique (CNRS).

Open access funding enabled and organized by Projekt DEAL.

Conflict of Interest

The authors declare no conflict of interest.

Data Availability Statement

The data that support the findings of this study are available at https://doi.org/10.17630/ceaea778-414a-4ef9-adf7-bdf228a42080 and in the repository Chemotion (https://www.chemotion-repository.net/). All DOIs minted for the data are linked to the specific experiments in the Supporting Infomation and a summary of all new data obtained in this study can be gained with the collection DOI https://dx.doi.org/10.14272/collection/JTS 2023-02-24 and https://dx.doi.org/10.14272/collection/JTS 2023-10-11.[29]

Keywords

carbazolophanes, circularly polarized luminescence, cyclophanes, organic light-emitting diodes, planar chirality, thermally activated delayed fluorescence

Received: January 31, 2024
Revised: April 7, 2024
Published online:

[1] a) M. Y. Wong, E. Zysman-Colman, *Adv. Mater.* **2017**, *29*, 1605444; b) Z. Yang, Z. Mao, Z. Xie, Y. Zhang, S. Liu, J. Zhao, J. Xu, Z. Chi, M. P. Aldred, *Chem. Soc. Rev.* **2017**, *46*, 915; c) G. Hong, X. Gan, C. Leonhardt, Z. Zhang, J. Seibert, J. M. Busch, S. Bräse, *Adv. Mater.* **2021**, *33*, 2005630.

[2] a) L. Frédéric, A. Desmarchelier, L. Favereau, G. Pieters, *Adv. Funct. Mater.* **2021**, *31*, 2010281; b) M. Li, C.-F. Chen, *Org. Chem. Front.* **2022**, *9*, 6441.

[3] a) J. M. Teng, D. W. Zhang, C. F. Chen, *ChemPhotoChem* **2022**, *6*, 202100228; b) S. Felder, M.-L. Delcourt, D. Contant, R. Rodríguez, L. Favereau, J. Crassous, L. Micouin, E. Benedetti, *J. Mater. Chem. C* **2023**, *11*, 2053.

[4] a) T. Niu, L. X. Liu, B. Wu, Y. G. Zhou, *J. Org. Chem.* **2023**, *88*, 7863; b) S. E. Gibson, J. D. Knight, *Org. Biomol. Chem.* **2003**, *1*, 1256; c) J. Paradies, *Synthesis* **2011**, *2011*, 3749; d) C. Zippel, Z. Hassan, M. Nieger, S. Bräse, *Adv. Synth. Catal.* **2020**, *362*, 3431; e) C. Braun, M. Nieger, S. Bräse, L. L. Schafer, *ChemCatChem* **2019**, *11*, 5264.

[5] a) Y. Morisaki, S. Shibata, Y. Chujo, *Can. J. Chem.* **2017**, *95*, 424; b) Y. Morisaki, Y. Chujo, *Polym. Chem.* **2011**, *2*, 1249; c) A. Morisaki, R. Inoue, Y. Morisaki, *Chemistry* **2023**, *29*, 202203533; d) K. Tanaka, R. Inoue, Y. Morisaki, *Chem. Asian J.* **2021**, *17*, 2021012.

[6] a) M. Cakici, Z. G. Gu, M. Nieger, J. Burck, L. Heinke, S. Bräse, *Chem. Commun.* **2015**, *51*, 4796; b) X. Xue, J. Wang, Q. Zhu, Y. Xue, H. Liu, *Dalton Trans.* **2021**, *50*, 1374; c) W. Gong, H. Xie, K. B. Idrees, F. A. Son, Z. Chen, F. Sha, Y. Liu, Y. Cui, O. K. Farha, *J. Am. Chem. Soc.* **2022**, *144*, 1826; d) Z. Shan, M. Wu, Z. Gu, Y. Nishiyama, G. Zhang, *Chem. Commun.* **2021**, *57*, 9236.

[7] a) T. Mohammadi Hafshejani, X. Zhong, J. Kim, B. Dadfar, J. Lahann, *Organic Mater.* **2023**, *5*, 98; b) D. Varadharajan, K. Nayani, C. Zippel, E. Spuling, K. C. Cheng, S. Sarangarajan, S. Roh, J. Kim, V. Trouillet, S. Bräse, N. L. Abbott, J. Lahann, *Adv. Mater.* **2022**, *34*, 2108386; c) T. Moss, A. Greiner, *Adv. Mater. Interfaces* **2020**, *7*, 1901858.
[8] Z. Hassan, E. Spuling, D. M. Knoll, J. Lahann, S. Brase, *Chem. Soc. Rev.* **2018**, *47*, 6947.
[9] E. Spuling, N. Sharma, I. D. W. Samuel, E. Zysman-Colman, S. Bräse, *Chem. Commun.* **2018**, *54*, 9278.
[10] M. Y. Zhang, Z. Y. Li, B. Lu, Y. Wang, Y. D. Ma, C. H. Zhao, *Org. Lett.* **2018**, *20*, 6868.
[11] M. Y. Zhang, X. Liang, D. N. Ni, D. H. Liu, Q. Peng, C. H. Zhao, *Org. Lett.* **2021**, *23*, 2.
[12] a) S. L. Buchwald, W. Huang, US2016359118A1, **2016**; b) N. Sharma, E. Spuling, C. M. Mattern, W. Li, O. Fuhr, Y. Tsuchiya, C. Adachi, S. Bräse, I. D. W. Samuel, E. Zysman-Colman, *Chem. Sci.* **2019**, *10*, 6689.
[13] A. K. Gupta, Z. Zhang, E. Spuling, M. Kaczmarek, Y. Wang, Z. Hassan, I. D. W. Samuel, S. Bräse, E. Zysman-Colman, *Mater. Adv.* **2021**, *2*, 6684.
[14] C. Liao, Y. Zhang, S. H. Ye, W. H. Zheng, *ACS Appl. Mater. Interfaces* **2021**, *13*, 25186.
[15] D. W. Zhang, J. M. Teng, Y. F. Wang, X. N. Han, M. Li, C. F. Chen, *Mater. Horiz.* **2021**, *8*, 3417.
[16] X. J. Liao, D. Pu, L. Yuan, J. Tong, S. Xing, Z. L. Tu, J. L. Zuo, W. H. Zheng, Y. X. Zheng, *Angew. Chem., Int. Ed.* **2023**, *62*, 202217045.
[17] a) T. Fan, Y. Zhang, L. Wang, Q. Wang, C. Yin, M. Du, X. Jia, G. Li, L. Duan, *Angew. Chem. Int. Ed. Engl.* **2022**, *61*, 202213585; b) H. Y. Zhou, D. W. Zhang, M. Li, C. F. Chen, *Angew. Chem. Int. Ed. Engl.* **2022**, *61*, 202117872; c) F. Wang, W. Qiu, J. Zeng, P. Yuan, W. Zong, W. Wu, Y. Liu, S. Xu, S.-J. Su, S. Cao, *J. Mater. Chem. C* **2020**, *8*, 4469; d) M. Hempe, A. K. Harrison, J. S. Ward, A. S. Batsanov, M. A. Fox, F. B. Dias, M. R. Bryce, *J. Org. Chem.* **2021**, *86*, 429; e) S. Izumi, H. F. Higginbotham, A. Nyga, P. Stachelek, N. Tohnai, P. Silva, P. Data, Y. Takeda, S. Minakata, *J. Am. Chem. Soc.* **2020**, *142*, 1482; f) W.-L. Zhao, Y.-F. Wang, S.-P. Wan, H.-Y. Lu, M. Li, C.-F. Chen, *CCS Chem.* **2022**, *4*, 3540; g) S. Shikita, G. Watanabe, D. Kanouchi, J. Saito, T. Yasuda, *Adv. Photonics Res.* **2021**, *2*, 2100021; h) Y. Hu, Z. Wang, X. Jiang, X. Cai, S. J. Su, F. Huang, Y. Cao, *Chem. Commun.* **2018**, *54*, 7850; i) Y. F. Wang, H. Y. Lu, Y. F. Shen, M. Li, C. F. Chen, *Chem. Commun.* **2019**, *55*, 9559.
[18] P. Lennartz, G. Raabe, C. Bolm, *J. of Chem.* **2012**, *52*, 171.
[19] a) T. Watanabe, S. Oishi, N. Fujii, H. Ohno, *J. Org. Chem.* **2009**, *74*, 4720; b) N. Yoshikai, Y. Wei, *Asian J. Org. Chem.* **2013**, *2*, 466.
[20] a) S. Patel, T. N. Dais, P. G. Plieger, G. J. Rowlands, *Beilstein J. Org. Chem.* **2021**, *17*, 1518; b) S. Biswas, Z. A. Tabasi, L. N. Dawe, Y. Zhao, G. J. Bodwell, *Org. Lett.* **2022**, *24*, 5009; c) S. Biswas, C. S. Qiu, L. N. Dawe, Y. Zhao, G. J. Bodwell, *Angew. Chem. Int. Ed. Engl.* **2019**, *58*, 9166; d) S. Biswas, Z. A. Tabasi, J. B. Lin, Y. Zhao, G. J. Bodwell, *Org. Lett.* **2021**, *23*, 5461; e) B. Ortner, R. Waibel, P. Gmeiner, *Angew. Chem. Int. Ed. Eng.* **2001**, *40*, 1283; f) N. De Rycke, J. Marrot, F. Couty, O. R. P. David, *Eur. J. Org. Chem.* **2011**, *2011*, 1980.
[21] K. Tani, K. Matsumura, K. Hori, Y. Tohda, H. Takemura, H. Ohkita, S. Ito, M. Yamamoto, *Chem. Lett.* **2002**, *31*, 934.
[22] T. Watanabe, S. Oishi, N. Fujii, H. Ohno, *J. Org. Chem.* **2009**, *74*, 4720.
[23] N. G. Connelly, W. E. Geiger, *Chem. Rev.* **1996**, *96*, 877.
[24] C. M. Cardona, W. Li, A. E. Kaifer, D. Stockdale, G. C. Bazan, *Adv. Mater.* **2011**, *23*, 2367.
[25] C. Han, Y. Zhao, H. Xu, J. Chen, Z. Deng, D. Ma, Q. Li, P. Yan, *Chem.-Eur. J.* **2011**, *17*, 5800.
[26] a) M. Cossi, N. Rega, G. Scalmani, V. Barone, *J. Comput. Chem.* **2003**, *24*, 669; b) V. Barone, M. Cossi, *J. Phys. Chem. A* **1998**, *102*, 1995. c) A. Klamt, G. Schüürmann, *J. Chem. Soc., Perkin Trans.* **1993**, *2*, 799.
[27] S. G. Ihn, N. Lee, S. O. Jeon, M. Sim, H. Kang, Y. Jung, D. H. Huh, Y. M. Son, S. Y. Lee, M. Numata, H. Miyazaki, R. Gomez-Bombarelli, J. Aguilera-Iparraguirre, T. Hirzel, A. Aspuru-Guzik, S. Kim, S. Lee, *Adv. Sci.* **2017**, *4*, 1600502.
[28] S. Diesing, L. Zhang, E. Zysman-Colman, I. D. W. Samuel, *Nature* **2024**, *627*, 747.
[29] Research data of this publication can be accessed as Open Access in the repository Chemotion. The data collection is assigned to and https://dx.doi.org/10.14272/collection/JTS_2023-10-11.